# Title: **Amide proton transfer-weighted imaging of pediatric brainstem glioma and its predicted value for H3 K27 alteration**

# Running title: APTw predicts H3 K27 alteration in pedBSG


## Abstract:

**Background**: Non-invasively determination of H3 K27 alteration of pediatric brainstem glioma (pedBSG) remains a clinical challenge.

**Purpose**: We aimed to predict H3 K27-altered pedBSG using amide proton transfer-weighted (APTw) imaging.

**Materials and methods**: This retrospective study included patients with pedBSG who underwent APTw imaging and had the H3 K27 alteration status determined by immunohistochemical staining. The presence or absence of foci of markedly increased APTw signal in the lesion was visually assessed. Quantitative APTw histogram parameters within the entire solid portion of tumors were extracted and compared between H3 K27-altered and wild-type groups using the Student's t-test. The ability of APTw for differential diagnosis was evaluated using logistic regression.

**Results**: Sixty pedBSG patients included 48 patients with H3 K27-altered tumor (age range 2-48 years) and 12 patients with wild-type tumor (age range 3-53 years). Visual assessment showed that the foci of markedly increased APTw signal intensity were more common in the H3 K27-altered group than in wild-type group (60% vs 16%, P = .007). Histogram parameters of APTw signal intensity in the H3 K27-altered group were significantly higher than those in the wild-type group (Median, 2.74% vs 2.22%, P = .02). The maximum (AUC =

0.72, P = .01) showed the highest diagnostic performance among histogram analysis. A combination of age, median, and maximum APTw signal intensity could predict H3 K27 alteration with a sensitivity of 81%, specificity of 75%, and AUC of 0.80.

**Conclusions**: APTw imaging may serve as an imaging biomarker for H3 K27 alteration of pedBSGs.

**Keywords**: Pediatric brainstem glioma; H3 K27 alteration; Amide proton transfer-weighted imaging; Histogram analysis.

## *Introduction*

Pediatric brainstem gliomas (pedBSGs) are a heterogeneous group of tumors that include H3 K27–altered tumors with a dismal prognosis and wide-type tumors cured with surgical resection with a benign prognosis (1–6). World Health Organization (WHO) 2021 criteria reclassified these into a newly defined entity, “Diffuse midline glioma, H3 K27-altered”, which occur primarily in children, but also in adults (7). The H3 K27 alteration status can serve as a qualified biomarker for diagnosis, prognosis, and therapeutic selection in pedBSG patients (6,8–11).

The invasive biopsy can identify the H3K27-altered status with high sensitivity and specificity but carries a significant risk of complication (12,13). However, the inter-tumoral heterogeneity of pedBSGs poses the risk of a biopsy bias. Routine clinical MRI is a non-invasive method to depict pedBSGs location, morphology, and diffusion characteristics. However, it cannot predict genetic alteration status based on the imaging appearance (14–16). Therefore, accurate non-invasive determination of H3 K27 alteration status in pedBSGs remains a clinical practice challenge.

Amide proton transfer-weighted (APTw) imaging is a molecular MRI technique that generates image contrast predominantly based on the amide protons in mobile cellular proteins and peptides endogenous in tissue (17). Previous studies in supratentorial gliomas demonstrated that a higher APTw value indicated a high protein and peptide metabolism level and was a potential radiological biomarkers for tumor characterizations, treatment

monitoring, and outcome prediction (18–25). However, no prior studies have reported the APTw characteristics of pedBSGs and their predicted value for H3 K27 alteration status.

This study aimed to investigate the APTw features of pedBSGs and its diagnostic value in predicting the H3 K27 alteration status.

## *Materials and methods*

### *Patients*

The Institutional Review Board of XXXX approved the retrospective study of brain APTw scans of consecutive patients with brain stem tumor prior to surgery or biopsy from December 2018 to October 2020 in XX hospital. The eligible criteria comprised (1) primary brainstem glioma; (2) known H3-K27 alteration and (3) preoperative APTw images. The exclusion criteria included (1) inadequate image quality; (2) secondary or multiple brain tumors **(Fig.1)**.

Clinical information, including age and gender, histopathology, and molecular features, was obtained from medical charts. Tumor grading was determined according to the 2021 WHO criteria (7). Molecular analyses of H3 K27 antibody and immunohistochemistry were performed to test the presence of alterations in the histone variants H3.3 (H3F3A) and H3.1(HIST1H3B) (26).

### *MRI acquisition*

MR imaging was carried out on a 3T MR scanner (Ingenia CX, Philips Healthcare, Best, the Netherlands). The protocol included T1-weighted imaging (T1w), T2-weighted imaging (T2w), fluid attenuated inversion recovery (FLAIR), and contrast-enhanced 3D T1w and APTw. Details of APTw protocols were as follows: 3D Turbo Spin Echo (TSE), repetition time (TR) = 5864 ms; echo time (TE)= 8.8 ms, flip angle (FA) = 90°, field of view=200

mm×200 mm, acquisition voxel size= 2 mm×2 mm×6 mm, slice number=7. A saturation pulse was applied at +3.5 ppm (relative to water protons) to saturate amide protons, saturation B1 amplitude=2uT, saturation duration=2s, parallel acceleration factor (SENSE) = 1.6, acquisition time = 1min54s. An unsaturated reference scan was obtained with otherwise similar acquisition parameters. The details of other sequences were shown in **Supplemental Table S1**.

### *APTw imaging calculation*

APTw maps were automatically calculated using the following post-processing pipeline on the MR console. An MTRasym analysis is conducted by a voxel-by-voxel analysis to distinguish the APT signal from several background effects (e.g., direct water saturation and magnetization transfer contributions from semi-solid tissue components). Firstly, the Z-spectrum is aligned per voxel using a B0 field map to locate the maximum direct water saturation exactly at 0 ppm. Secondly, the asymmetry is calculated by subtracting the positive frequency side $S[+\Delta\omega]$ from the negative side $S[-\Delta\omega]$ and normalized to the unsaturated image S0 (See Equation 1). The resulting MTRasym value at +3.5 ppm is presented as percent level (relative to S0) in the final APTw images (Equation 2).

$$MTR_{asym}(\%) = (S_{-\Delta\omega} - S_{+\Delta\omega})/S_0 \text{ (Equation 1)}$$

$MTR_{asym}(\%)$ = Magnetization Transfer Ratio asymmetry in percent, $S_{-\Delta\omega}$ = signal at negative frequency offset $-\Delta\omega$, $S_{+\Delta\omega}$ = signal at positive frequency offset $+\Delta\omega$, $S_0$ = signal without radio frequency saturation.

$$APT_w\% = MTR_{asym}[\Delta\omega = +3.5ppm](\%) \text{(Equation 2)}$$

$APT_w\%$ = Amide Proton Transfer weighted percentage, $MTR_{asym}[\Delta\omega = +3.5ppm](\%)$ = Magnetization Transfer Ratio asymmetry at +3.5ppm offset frequency.

### *Visual assessment*

All APTw images were visually assessed using MRIcroN software (http://www.nitrc.org/projects/mricron) that allows a pseudocolor display (model: NIH, range: -10 to 15). Two neuroradiologists (D. C. and L. Q., both with three years' experience in neuroradiology), who were blinded to all clinical details, including age, gender and histopathological report, evaluated routine MRI appearances including edema, cystic or necrosis component, contrast enhancement, and the APTw appearance independently. We also performed the visual assessment of APTw appearance aiming to correlate it with molecular subtypes and compare with quantitative analysis of histogram parameters. The neuroradiologists were first trained based on 10 cases (randomly selected by a third observer [Y. D. with 12 years' experience in neuroradiology]) before performing the visual assessments. The tumors were evaluated for APTw hyperintensity (displayed as red to yellow) in the APTw image, relative to normal background signal in normal-appearing white mater (green to blue).(27) Assessment of APTw signal intensity within the tumor was performed according to the presence or absence of the clearly increased signal intensity (red areas) in any area of the tumor except necrosis and cysts.

### *Quantitative imaging analysis*

Tumor masks were manually drawn by two radiologists (D. C. and L. Q.) who were blinded to the clinical data based on axial 2D T2w images, using other sequences (including T1w, FLAIR, contrast-enhanced T1w) as reference. Tumor segmentation was performed using 3D Slicer (version 4.10.2) (28). The masks were carefully checked to ensure the solid tumor tissue inclusion, avoiding cystic, large necrotic, or hemorrhagic areas (21,29). Finally, the overlapping regions of the tumor masks drawn by the two radiologists (modified by the third radiologist [Y. D.] if necessary) were used for the quantitative analysis. The tumor masks were warped onto the APTw images by transformation parameters derived from the affine registration of T2w images to the unsaturated APTw source image.

Histogram parameters including median, maximum, minimum, 95% quantile, 75% quantile, 25% quantile, and 5% quantile, of the APTw signal intensity within the tumor were extracted.

### *Statistical analysis*

The statistical analysis was performed using R software (R version 4.2.2; R Project for Statistical Computing, http://www.r-project.org).

Categorical variables were described with frequencies and tested by Chi-square test. Continuous variables were expressed as mean and standard deviation (SD) and tested by Student's t-test. Interobserver agreement for APTw visual assessment was assessed by using the Kappa statistic. Univariable and multivariable logistic regression analyses were

performed to explore the ability of APTw signal intensity to predict the H3 K27 alteration status. Classification accuracy, sensitivity, specificity, and area under the receiver operating characteristic curve (AUC) were used to evaluate the model performance. Cutoff values were determined by maximizing the Youden index. The survival analysis was conducted using the univariate Kaplan–Meier method. A *P* value < .05 was deemed as statistically significant.

## *Results*

### *Patient characteristics*

Initially, 65 patients with primary pedBSG were identified. Five patients (one with multiple tumors, four with inadequate image quality) were excluded. Finally, 60 pedBSG patients including 48 patients with the H3 K27 alteration tumor (aged 12.10 ± 10.55 y; range, 2-48 y; male/female=21/27) and 12 patients with wild-type tumor (aged 26.42 ± 21.11 y; range, 3-53 y; male/female=9/3) were included in this study (**Table 1**). No significant difference in gender was observed between the H3 K27-altered group and the wild-type group. The patients in the H3 K27-altered group were on average roughly half as old as than those in the wild-type group ($P$ = .001).

### *Routine MRI characteristics and histopathological findings*

No difference was observed between H3 K27-altered and wild-type patients for conventional MRI characteristics (e.g., edema, cystic or necrosis component, contrast enhancement). All of H3 K27-altered pedBSG patients presented with WHO grade 4 tumors (48 [100%] vs 1 [8.33%]; $P$ < .001), while 8 (66.67%) of wild-type pedBSG cases presented with WHO grade 2 tumors (**Table 1**).

### *APTw characteristics*

All pedBSGs demonstrated heterogeneous signals on the APTw images. The Kappa coefficient assessing interobserver agreement for the occurrence of a focus of visually increased local APTw signal intensity between the two readers was 0.83 ($P$ <.001). Discordant results were resolved by the third senior neuroradiologist for further analyses. Of the 48 cases with H3 K27-altered pedBSG, 29 (60.41%) patients had areas of increased APTw signal intensity (red areas on the APTw images), which identified in only 2 (16.67%) of 12 cases in the wild-type group ($P$ = .007). Representative images of H3 K27-altered and wild-type pedBSGs are shown in **Fig.2**.

Higher median, maximum, 95% quantile and 75% quantile APTw signal intensity were observed in patients with H3 K27-altered tumors compared to those with H3 K27 wild-type tumors ($P$ <0.05) **(Fig.3A)**. Minimum, 25% quantile, and 5% quantile of APTw signal intensity showed no differences between the two groups.

### *Prediction of H3 K27 alteration in pedBSG*

We first conducted the prediction of H3 K27 alteration status using the presence of an area of increased APTw signal for a comparison with the APTw histogram parameters. The presence of an area of increased APTw signal intensity achieved an accuracy of 65% (39/60), sensitivity of 60% (29/48), and specificity of 83% (10/12). When combined with age, the

performance was not significantly improved with an accuracy of 63% (38/60), sensitivity of 54% (26/48), specificity of 100% (12/12), and AUC of 78% was obtained **(Fig.3B).**

For APTw histogram parameters, the univariate logistic analysis showed that median, maximum, 95% quantile and 75% quantile were better predictors of H3 K27-altered tumors (AUCs = 0.70 - 0.72, *P* = .01- .04) compared to minimum, 25% quantile and 5% quantile(AUCs = 0.47 - 0.63, *P* = .09 - .73) (Table 2). Considering the maximum, 95% quantile and 75% quantile indicate similar biology, which was a high level of amide proton concentration within a tumor, and the maximum had the highest AUC and the most statistical significance (AUC = 0.72, P = .01) for the prediction; finally, median and maximum APTw signal intensity and age were selected as the variates in the multivariable logistic regression analysis. Result showed an accuracy of 80% (48/60), sensitivity of 81% (39/48), specificity of 75% (9/12), and AUC of 80% **(Fig.3B)**.

***Survival Analysis***

43 patients were included in the survival analysis, while 17 patients were lost to follow-up after surgery. For these patients, the median overall survival (OS) of the H3 K27-altered group was 10.6 months, while more than half of patients in the wild-type group (7/9) were alived until the last follow-up (P < 0.0001) **(Fig.4)**.

## *Discussion*

In the present study, APTw imaging features in pedBSG were found to differ between H3 K27-altered and wild-type tumors. The main findings were as follows: (1) the presence of a focus of clearly increased signal (red areas) by the visual assessment on APTw is highly specific for pedBSG patients with the H3 K27 alteration; (2) higher median, maximum, 95% and 75% quantile APTw signal intensity in the H3 K27-altered pedBSG were observed compared to wild-type cases; (3) A combination of age, the median, and maximum APTw value within the tumor could accurately predict the H3 K27 alteration.

In our sample of 60 cases, younger ages in H3 K27-altered pedBSG patients were observed compared to H3 K27 wild-type, and no gender difference between the two groups was identified, consistent with previous evidence (14). The conventional radiographic features of pedBSG, including edema, cyst or necrosis, and contrast enhancement, showed no differences between the two groups, confirming the difficulty of predicting the H3 K27 alteration status based on routine MRI, as noted in previous studies (15,30).

The presence of focally increased APTw signal intensity (displayed as red on APTw images) was observed by 60.41% of pedBSG patients with the H3 K27 alteration by visual assessment. For differentiation of the two groups, a high specificity (100%) of the combination of age and presence of the highest APTw signal intensity was achieved to predict the H3 K27 alteration, implying a simple way to identify pedBSG with H3 K27

alteration. However, the sensitivity of visual assessment predicting the H3 K27 alteration is relatively low (54%), suggesting suboptimal model performance.

Quantitative analysis revealed higher APTw median but especially extreme values (e.g., maximum, 95% quantile, and 75% quantile) in pedBSG patients with the H3 K27 alteration, indicating that this alteration of tumor cells may associate with foci containing a high concentration of mobile protein and peptides, as lower overall amounts of H3 with trimethylated lysine (H3 K27me3) leading to increased cell proliferation (31–33). For identification of the H3 K27 alteration in pedBSGs, a combination of quantitative APTw measures (median and maximum APTw signal intensity) and age achieved an AUC (0.80), sensitivity (81%) and specificity (75%), and the combination of the presence of the highest ATPw signal by visual assessment and age (sensitivity: 54% and specificity:100%) presented a high specificity, indicating that APTw imaging could be a promising radiological biomarker to predict the H3 K27 alteration status.

In the survival analysis, we observed a significant difference in OS between the 2 groups indicating that that H3 K27 alteration status was predictive of OS in both groups, which is in line with previous work (9,34).

There are some limitations. First, our findings are based on retrospective data from a single center with a relatively small sample size, which is not applicable to independent test or cross

validation; a prospective multi-center study recruiting large samples is warranted to validate the generalizability. Second, the advanced conventional machine learning and deep learning algorithms have the potential power to improve predictive accuracy, which would be furtherly investigated in our subsequent studies. Third, we did not include other advanced MR imaging techniques, such as MR spectroscopy and diffusion-weighted imaging, which may add more value to the prediction model.

In conclution, the presence of the locally increased ATPw signal by visual assessment is highly specific for pedBSGs with the H3 K27 alteration. Higher APTw signal intensity were related to H3 K27 alteration in pedBSG. APTw imaging may serve as an imaging biomarker for H3 K27 alteration of pedBSGs .

**References:**

1. Wu G, Broniscer A, McEachron TA, et al. Somatic histone H3 alterations in pediatric diffuse intrinsic pontine gliomas and non-brainstem glioblastomas. Nat Genet 2012;44:251–253.

2. Chan K-M, Fang D, Gan H, et al. The histone H3.3K27M mutation in pediatric glioma reprograms H3K27 methylation and gene expression. Genes Dev 2013;27:985–990.

3. Funato K, Major T, Lewis PW, et al. Use of human embryonic stem cells to model pediatric gliomas with H3.3K27M histone mutation. Science 2014;346:1529–1533.

4. Nikbakht H, Panditharatna E, Mikael LG, et al. Spatial and temporal homogeneity of driver mutations in diffuse intrinsic pontine glioma. Nat Commun 2016;7:11185.

5. Leach JL, Roebker J, Schafer A, et al. MR imaging features of diffuse intrinsic pontine glioma and relationship to overall survival: report from the International DIPG Registry. Neuro-Oncology 2020;22:1647–1657.

6. Saratsis AM, Kambhampati M, Snyder K, et al. Comparative multidimensional molecular analyses of pediatric diffuse intrinsic pontine glioma reveals distinct molecular subtypes. Acta Neuropathol 2014;127:881–895.

7. Louis DN, Perry A, Wesseling P, et al. The 2021 WHO Classification of Tumors of the Central Nervous System: a summary. Neuro Oncol 2021;noab106.

8. Nagaraja S, Vitanza NA, Woo PJ, et al. Transcriptional Dependencies in Diffuse Intrinsic Pontine Glioma. Cancer Cell 2017;31:635-652.e6.

9. Khuong-Quang D-A, Buczkowicz P, Rakopoulos P, et al. K27M mutation in histone H3.3 defines clinically and biologically distinct subgroups of pediatric diffuse intrinsic pontine gliomas. Acta Neuropathol 2012;124:439–447.

10. Louis DN, Perry A, Reifenberger G, et al. The 2016 World Health Organization Classification of Tumors of the Central Nervous System: a summary. Acta Neuropathol 2016;131:803–820.

11. Chung C, Sweha SR, Pratt D, et al. Integrated Metabolic and Epigenomic Reprograming by H3K27M Mutations in Diffuse Intrinsic Pontine Gliomas. Cancer Cell 2020;38:334-349.e9.

12. Williams JR, Young CC, Vitanza NA, et al. Progress in diffuse intrinsic pontine glioma: advocating for stereotactic biopsy in the standard of care. Neurosurgical Focus 2020;48:E4.

13. Tejada S, Aquilina K, Goodden J, et al. Biopsy in diffuse pontine gliomas: expert neurosurgeon opinion—a survey from the SIOPE brain tumor group. Childs Nerv Syst 2020;36:705–711.

14. Chiang J, Diaz AK, Makepeace L, et al. Clinical, imaging, and molecular analysis of pediatric pontine tumors lacking characteristic imaging features of DIPG. Acta Neuropathologica Communications 2020;8:57.

15. Aboian MS, Solomon DA, Felton E, et al. Imaging Characteristics of Pediatric Diffuse Midline Gliomas with Histone H3 K27M Mutation. American Journal of Neuroradiology 2017;38:795–800.

16. Thust S, Micallef C, Okuchi S, et al. Imaging characteristics of H3 K27M histone-mutant diffuse midline glioma in teenagers and adults. Quant Imaging Med Surg 2021;11:43–56.

17. Zhou J, Lal B, Wilson DA, et al. Amide proton transfer (APT) contrast for imaging of brain tumors. Magn Reson Med 2003;50:1120–1126.

18. Togao O, Yoshiura T, Keupp J, et al. Amide proton transfer imaging of adult diffuse gliomas: correlation with histopathological grades. Neuro-Oncology 2014;16:441–448.

19. Park JE, Kim HS, Park KJ, et al. Pre- and Posttreatment Glioma: Comparison of Amide Proton Transfer Imaging with MR Spectroscopy for Biomarkers of Tumor Proliferation. Radiology 2016;278:514–523.

20. Su C, Liu C, Zhao L, et al. Amide Proton Transfer Imaging Allows Detection of Glioma Grades and Tumor Proliferation: Comparison with Ki-67 Expression and Proton MR Spectroscopy Imaging. AJNR Am J Neuroradiol 2017;38:1702–1709.

21. Park JE, Kim HS, Park SY, et al. Identification of Early Response to Anti-Angiogenic Therapy in Recurrent Glioblastoma: Amide Proton Transfer–weighted and Perfusion-weighted MRI compared with Diffusion-weighted MRI. Radiology 2020;295:397–406.

22. Suh CH, Park JE, Jung SC, et al. Amide proton transfer-weighted MRI in distinguishing high- and low-grade gliomas: a systematic review and meta-analysis. Neuroradiology 2019;61:525–534.

23. Jiang S, Eberhart CG, Lim M, et al. Identifying Recurrent Malignant Glioma after Treatment Using Amide Proton Transfer-Weighted MR Imaging: A Validation Study with Image-Guided Stereotactic Biopsy. Clin Cancer Res 2019;25:552–561.

24. Sotirios B, Demetriou E, Topriceanu CC, et al. The role of APT imaging in gliomas grading: A systematic review and meta-analysis. Eur J Radiol 2020;133:109353.

25. Paech D, Windschuh J, Oberhollenzer J, et al. Assessing the predictability of IDH mutation and MGMT methylation status in glioma patients using relaxation-compensated multipool CEST MRI at 7.0 T. Neuro Oncol 2018;20:1661–1671.

26. Bechet D, Gielen GGH, Korshunov A, et al. Specific detection of methionine 27 mutation in histone 3 variants (H3K27M) in fixed tissue from high-grade astrocytomas. Acta Neuropathol 2014;128:733–741.

27. Zhao X, Wen Z, Huang F, et al. Saturation Power Dependence of Amide Proton Transfer (APT) Image Contrasts in Human Brain Tumors and Strokes at 3T. Magn Reson Med 2011;66:1033–1041.

28. Fedorov A, Beichel R, Kalpathy-Cramer J, et al. 3D Slicer as an Image Computing Platform for the Quantitative Imaging Network. Magn Reson Imaging 2012;30:1323–1341.

29. Park JE, Kim HS, Park KJ, et al. Histogram Analysis of Amide Proton Transfer Imaging to Identify Contrast-enhancing Low-Grade Brain Tumor That Mimics High-Grade Tumor: Increased Accuracy of MR Perfusion. Radiology 2015;277:151–161.

30. Hoffman LM, Veldhuijzen van Zanten SEM, Colditz N, et al. Clinical, Radiologic, Pathologic, and Molecular Characteristics of Long-Term Survivors of Diffuse Intrinsic Pontine Glioma (DIPG): A Collaborative Report From the International and European Society for Pediatric Oncology DIPG Registries. JCO 2018;36:1963–1972.

31. Lewis PW, Muller MM, Koletsky MS, et al. Inhibition of PRC2 Activity by a Gain-of-Function H3 Mutation Found in Pediatric Glioblastoma. Science 2013;340:857–861.

32. Wu Y, Zhou IY, Lu D, et al. pH-sensitive amide proton transfer effect dominates the magnetization transfer asymmetry contrast during acute ischemia-quantification of multipool contribution to in vivo CEST MRI: Resolution of Multipool Contribution to In Vivo pH-Sensitive APT MRI. Magn Reson Med 2018;79:1602–1608.

33. Larson JD, Kasper LH, Paugh BS, et al. Histone H3.3 K27M Accelerates Spontaneous Brainstem Glioma and Drives Restricted Changes in Bivalent Gene Expression. Cancer Cell 2019;35:140-155.e7.

34. Su X, Chen N, Sun H, et al. Automated machine learning based on radiomics features predicts H3 K27M mutation in midline gliomas of the brain. Neuro-Oncology 2019;noz184.

**Figure legends**

**Fig.1** Flowchart of the retrospective cohort for H3 K27 alternation prediction in this study.

**Fig.2** MRI features of pedBSG patients with H3 K27-altered and wild-type. Row 1. a 28-year-old female diagnosed with H3 K27 wild-type tumor (WHO grade 2) shows no foci of increased signal intensity on APTw image; Row 2. a 3-year-old boy diagnosed with wild-type tumor (WHO grade 2) tumor without increased signal intensity on APTw image; Row 3. a 4-year-old boy diagnosed with H3 K27-altered diffuse pontine glioma (WHO grade 4) presents an extensive area of increased signal intensity (displayed as red) on APTw image; Row 4. A32 year-old female diagnosed with H3 K27-altered tumor (WHO grade 4) presents with a small focus of clearly increased signal intensity (displayed as red) on the APTw image. Sag, sagittal; Ax, axial; R, right

**Fig.3** (A) Box plots of Age, APTw median, maximum, 95% quantile and 75% quantile according to H3 K27 status (H3 K27-altered and wild-type), (B) Diagnostic performance of the amide proton transfer-weighted (APT) parameters in differentiating theH3 K27 status of pedBSGs. APTw, amide proton transfer weighted; AUC, area under the curve; ROC, Receiver Operating Characteristic

**Fig.4** Overall survival analysis of H3 K27-altered group and wild-type group.

**Table 1**. Demographic and conventional MRI characteristics of pedBSG patients

| | PedBSG Patients (n=60) | H3 K27-altered Group (n=48) | Wild-type Group (n=12) | *P*-value |
|---|---|---|---|---|
| Age, y | | | | |
| Mean ± SD | 14.97 ± 14.32 | 12.10 ± 10.55 | 26.42 ± 21.11 | .001 |
| Range | 2-53 | 2-48 | 3-53 | |
| Gender | | | | .24 |
| Male, n (%) | 30 (50%) | 21 (43.75%) | 9 (75.00%) | |
| Female, n (%) | 30 (50%) | 27 (56.25%) | 3 (25.00%) | |
| MRI characteristics | | | | |
| Edema, n (%) | 11 (26.67%) | 9 (18.75%) | 2 (16.67%) | .87 |
| Cyst or necrosis, n (%) | 33 (55%) | 19 (40.43%) | 4 (33.33%) | .65 |
| Contrast enhancement, n (%) | 34/54* (62.96%) | 26 (61.90%) | 8 (66.67) | .77 |
| Histopathology (WHO Grade) | | | | <.001 |
| 2, n (%) | 8 (13.33%) | 0 | 8 (66.67%) | |
| 3, n (%) | 3 (0.05%) | 0 | 3 (25.00%) | |
| 4, n (%) | 49 (81.67%) | 48 (100%) | 1 (8.33%) | |

*54/60 patients had contrast-enhanced 3D T1w.

*P*-values for the comparison between H3 K27-altered and wild-type groups.

Abbreviations: pedBSG, pediatric brainstem glioma; WHO, World Health Organization; SD, standard deviation;

n, number.

**Table 2**. Age and APTw characteristics of pedBSG patients and corresponding predicting performance for H3 K27 alteration status

| | H3 K27-altered Group (n=48) | Wild-type Group (n=12) | *P*-value | Cutoff value | Accuracy | Sensitivity (%) | Specificity (%) | AUC |
|---|---|---|---|---|---|---|---|---|
| Age (mean ± SD,y) | 12.10 ± 10.55 | 26.42 ± 21.11 | .001 | 23.00 | 0.80 | 85 | 58 | 0.60 |
| Foci of markedly increased APTw signal intensity, n (%) | 29 (60.41%) | 2 (16.67%) | .007 | | 0.65 | 60 | 83 | |
| Histogram parameters | | | | | | | | |
| Median (mean ± SD) | 2.74 ± 0.66 | 2.22 ± 0.65 | .02 | 1.99 | 0.87 | 96 | 50 | 0.72 |
| Maximum (mean ± SD) | 7.54 ± 2.06 | 5.85 ± 2.01 | .01 | 5.95 | 0.73 | 75 | 67 | 0.72 |
| Minimum (mean ± SD) | 0.11 ± 0.42 | 0.15 ± 0.31 | .73 | 0.01 | 0.78 | 88 | 42 | 0.60 |
| 95% quantile (mean ± SD) | 5.03 ± 1.69 | 3.96 ± 0.87 | .04 | 5.16 | 0.50 | 38 | 100 | 0.70 |
| 75% quantile (mean ± SD) | 3.61 ± 0.99 | 2.90 ± 0.68 | .02 | 2.55 | 0.87 | 96 | 50 | 0.72 |
| 25% quantile (mean ± SD) | 1.94 ± 0.55 | 1.63 ± 0.62 | .09 | 1.48 | 0.72 | 77 | 50 | 0.63 |
| 5% quantile (mean ± SD) | 0.93 ± 0.62 | 0.84 ± 0.54 | .62 | 0.86 | 0.55 | 54 | 58 | 0.47 |

Abbreviations: SD, standard deviation; APTw, amide proton transfer-weighted; AUC, area under the curve.

Figure 1

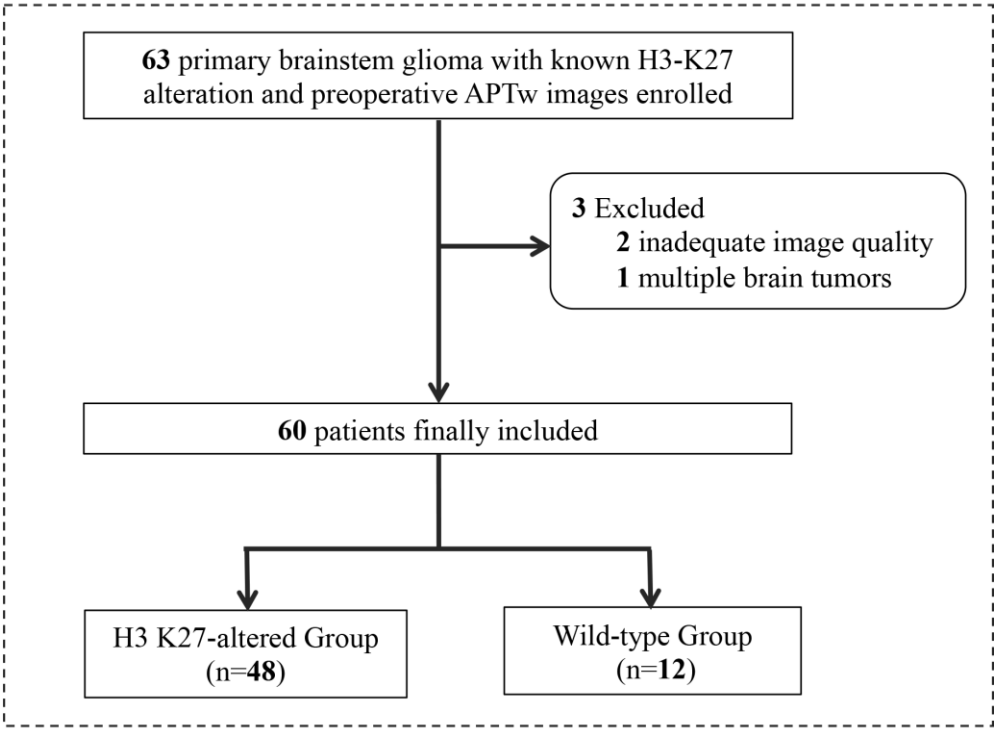
63 primary brainstem glioma with known H3-K27 alteration and preoperative APTw images enrolled
3 Excluded
2 inadequate image quality
1 multiple brain tumors
60 patients finally included
H3 K27-altered Group (n=48)
Wild-type Group (n=12)

Figure 2

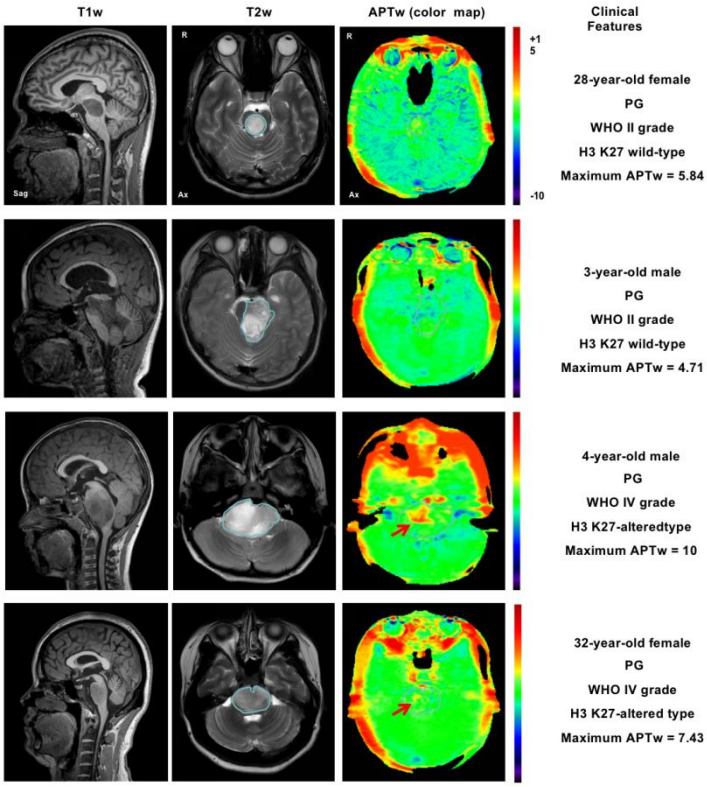
T1w
T2w
APTw (color map)
Clinical Features
+1
5
-10
Sag
Ax
Ax
R
R
28-year-old female
PG
WHO II grade
H3 K27 wild-type
Maximum APTw = 5.84
3-year-old male
PG
WHO II grade
H3 K27 wild-type
Maximum APTw = 4.71
4-year-old male
PG
WHO IV grade
H3 K27-alteredtype
Maximum APTw = 10
32-year-old female
PG
WHO IV grade
H3 K27-altered type
Maximum APTw = 7.43

Figure 3

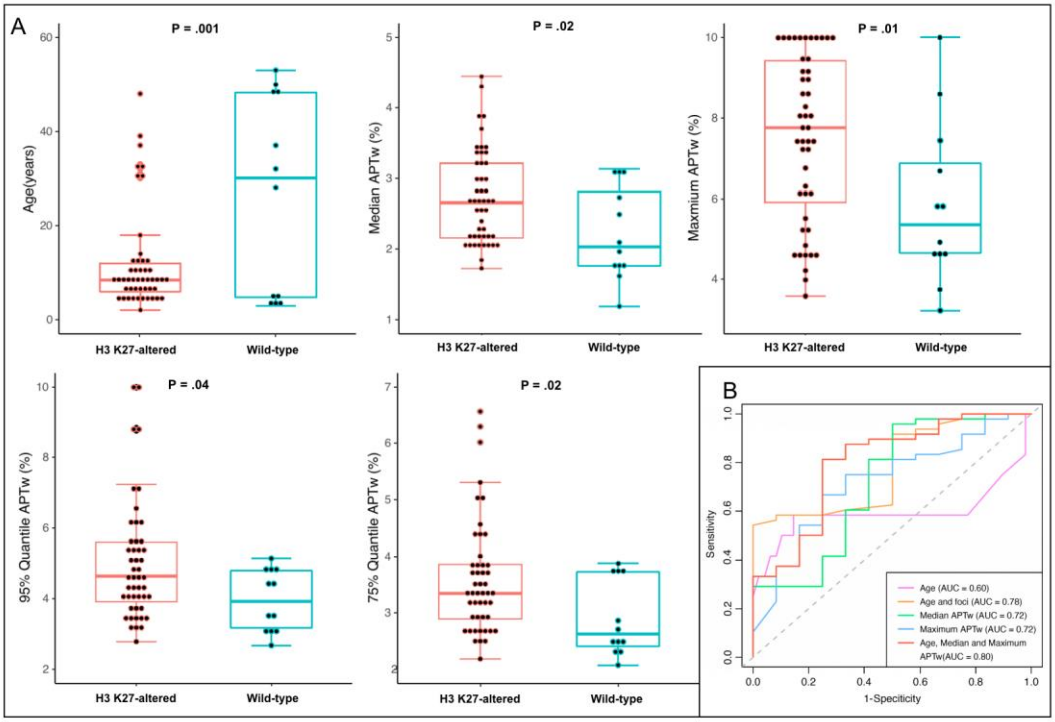
A
P = .001
Age(years)
H3 K27-altered
Wild-type
P = .02
Median APTw (%)
P = .01
Maxmium APTw (%)
P = .04
95% Quantile APTw (%)
P = .02
75% Quantile APTw (%)
B
Sensitivity
1-Speciticity
Age (AUC = 0.60)
Age and foci (AUC = 0.78)
Median APTw (AUC = 0.72)
Maximum APTw (AUC = 0.72)
Age, Median and Maximum APTw(AUC = 0.80)

Figure 4

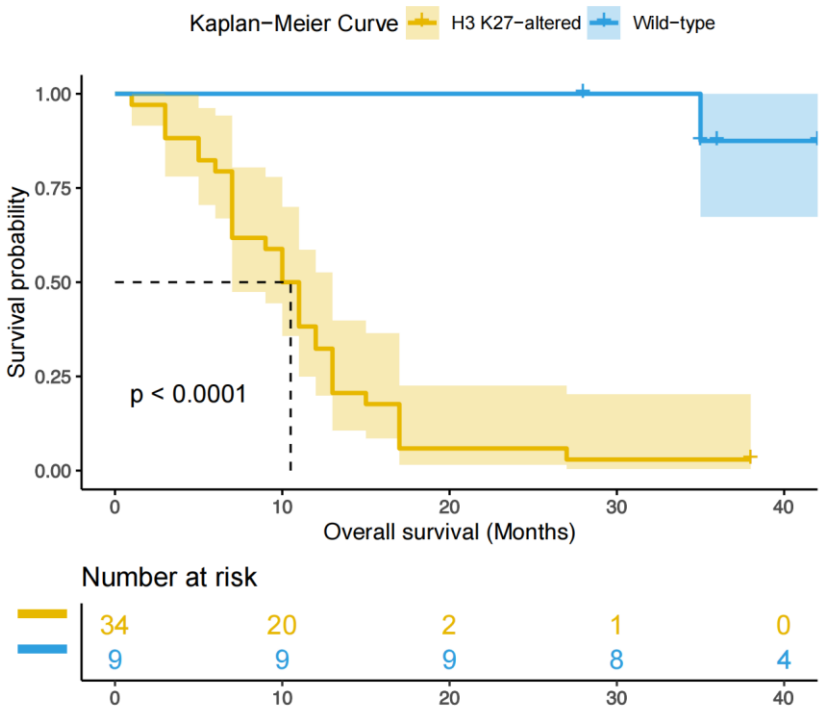
Kaplan−Meier Curve
H3 K27−altered
Wild−type
Survival probability
1.00
0.75
0.50
0.25
0.00
p < 0.0001
0
10
20
30
40
Overall survival (Months)
Number at risk
34
20
2
1
0
9
9
9
8
4
0
10
20
30
40

## Supplement materials

Table S1. MRI protocols of T1w, T2w, FLAIR, and contrast-enhanced T1w.

| Protocols | Sequence | FA (degree) | TR (ms) | TE (ms) | IR (ms) | Acquisition voxel size (mm3) | In-plane acquisition matrix | Slice number | Acquisition time |
|---|---|---|---|---|---|---|---|---|---|
| T1w (sag) | 3D TFE | 8 | 6.6 | 3 | | 1×1×1 | 256×256 | 196 | 2min20s |
| T2w (ax) | 2D TSE | 90 | 2800 | 135 | | 1×1×5 (gap 0.5mm) | 240×240 | 24 | 1min |
| T2-FLAIR (sag) | 3D TSE | 90 | 4800 | 340 | 1605 | 1×1×1 | 240×240 | 180 | 2min28s |
| Contrast-enhanced T1w (sag) | 3D TFE | 8 | 6.6 | 3 | | 1×1×1 | 256×256 | 196 | 2min20s |

Abbreviations: FA, flip angle; TR, repetition time; TE, echo time; IR, inversion recovery; FLAIR, fluid-attenuated inversion recovery; TFE, turbo field echo; TSE, turbo spin-echo; sag, sagittal; ax, axial.